Control of Powder Microstructure for Improved Infrared Reflectance Modulation of an Electrochromic Plastic Device

A. Bessière,[†,‡] L. Beluze,[†,§] M. Morcrette,[§] V. Lucas,[‡] B. Viana,*[,†] and J.-C. Badot[†]

LCAES, UMR 7574, ENSCP 11 Rue Pierre & Marie Curie, 75231 Paris Cedex 05, France, EADS CCR, 12 Rue Pasteur BP 76, 92152 Suresnes Cedex, France, and LRCS, UMR 6007, 33 rue Saint Leu, 80039 Amiens Cedex, France

Received December 20, 2002. Revised Manuscript Received April 10, 2003

The so-called plastic technology first developed for Li-ion batteries is demonstrated for its potential optical applications in infrared emissivity control. $WO_3 \cdot H_2O$ powder embedded in a plastic matrix is used as the active component in the $LiCoO_2$/Li electrolyte/$WO_3 \cdot H_2O$ system. The role of the microstructure of $WO_3 \cdot H_2O$ as an electrochromic material is investigated. For instance, platelet-shaped grains with a surface area as large as 15 μm^2 induce a large improvement in device contrast properties. Reflectance measurements show a 53% contrast between the bleached and colored states over the 8−12 μm range. This effect is likely rooted in the free electron mobility in addition to scattering and phonon effects. The optical modulation performance over the range 2.5−20 μm compares favorably with literature results on solid devices built from annealed and sputtered *m*-WO_3 thin films.

Introduction

Recently, there has been growing interest in emissivity modulators because they represent a clever way to control thermal exchange without expending energy.[1] With electrochromic (EC) reflectance modulators, a very small current output induces a surface switch from an absorbing to a reflecting state for incident radiation. This is of particular importance in satellite thermal control, where heavy louver-type radiators[2−4] are still used to regulate the radiation transfer in the same way as a venetian blind. In the past decade, some rigid EC devices based on monoclinic tungsten oxide have been built;[5−9] their infrared (IR) switching properties have been investigated in an effort to increase the reflectance contrast.[10−18] The trend now is a search for plastic devices that would present tremendous advantages over rigid ones.[19] Flexible devices could adjust to components with complex shapes; in addition, their low weight would result in great energy savings, especially for satellites. That is the reason why some recent experiments supported by NASA were carried out along this direction. Within such experiments, some solid-state (germanium-based) EC tiles were put on a Kapton plastic substrate and integrated into a multifunctional composite structure.[20] The structure incorporates nine 5-cm^2 EC tiles, which can exhibit a 15% emissivity variation over the 8−12 μm range within 15 min. However, a bending test performed on the entire device was unsuccessful, leading to cracking of the germanium substrate supporting the solid-state tiles; thus, there is still a need for a completely flexible device.

In a previous work, we reported the performance of a flexible EC infrared (IR) emittance device based on

* Corresponding author. Tel.: (33) 01 44 27 67 08. Fax (33) 01 46 34 74 89. E-mail: viana@ext.jussieu.fr.
† LCAES.
‡ EADS CCR.
§ LRCS.

(1) Granqvist, C. G. *Materials Science for Solar Energy Conversion Systems*; Pergamon Press: Elmsford, NY, 1991.
(2) Trimble, C.; Devries, M.; Hale, J. S.; Thompson, D. W.; Tiwald, T. E.; Woollam, J. A. *Thin Solid Films* **1999**, *26*, 355.
(3) Larsson, A. L.; Niklasson, G.; Stenmark, L. *Proc. SPIE* **1999**, *3738*, 486.
(4) Hale, J. S.; Devries, M.; Dworak, B.; Woollam, J. A. *Thin Solid Films* **1998**, *205*, 313.
(5) Goldner, R. B.; Mendelsohn, D. H.; Alexander, J.;. Henderson, W. R.; Fitzpatrick, D.; Hasas, T. E.; Sample, H. H.; Rauh, R. D.; Parker, M. A.; Rose, T. L. *Appl. Phys. Lett.* **1983**, *43* (12), 1093.
(6) Mendelsohn, D. H.; Goldner, R. B. *J. Electrochem. Soc.* **1984**, *131*, 857.
(7) Goldner, R. B., Norton, P.; Wong, K.; Foley, G.; Goldner, E. L.; Seward, G.; Chapman, R. *Appl. Phys. Lett.* **1985**, *47* (5), 536.
(8) Cogan, S. F.; Plante, T. D.; Parker, M. A.; Rauh, R. D. *J. Appl. Phys.* **1986**, *60* (8), 2735.
(9) Devries, M. J.; Trimble, C.; Tiwald, T. E.; Thompson, D. W.; Woollam, J. A.; Hale, J. S. *J. Vac. Sci. Technol.* **1999**, *5A*, 517.
(10) Goldner, R. B.; Rauh, R. D. *Proc. SPIE* **1983**, *428*, 38.
(11) Goldner, R. B.; Brofos, A.; Foley, G.; Goldner, E. L.; Haas, T. E.; Henderson, W.; Norton, P.; Ratnam, B. A.; Weis, N.; Wong, K. K. *Sol. Energy Mater.* **1995**, *12*, 403.
(12) Cogan, S. F.; Anderson, E. J.; Plante, T. D.; Rauh, R. D. *Proc. SPIE* **1985**, *562*, 23.
(13) Berera, G.; Goldner, R. B.; Arntz, F. O.; Wong, K. K.; Ciaccia, A.; Welch, M.; Haas, T. E.; Jauniskis, L. *Mater. Res. Soc. Symp. Proc.* **1991**, *210*, 69.
(14) Cogan, S. F.; Rauh, R. D.; Westwood, J. D.; Plotkin, D. I.; Jones, R. B. *Proc. SPIE* **1989**, *2*, 1149.
(15) Cogan, S. F.; Rauh, R. D.; Klein, J. D.; Plante, T. D. In *Proceedings of the Symposium on Electrochromic Materials II*; The Electrochemical Society, Inc.: Pannington, NJ, 1995; Vol. 94-2, p 269.
(16) Hale, J. S.; Woollam, J. A. *Thin Solid Films* **1999**, *339*, 174.
(17) Franke, E. B.; Trimble, C. L.; Hale, J. S.; Schubert, M.; Woollam, J. A. *J. Appl. Phys.* **2000**, *88* (10), 5777.
(18) Franke, E. B.; Trimble, C. L.; Schubert, M.; Woollam, J. A.; Hale, J. S. *Appl. Phys. Lett.* **2000**, *77* (7), 930.
(19) O'Brien, N.; Gordon, J.; Mathew, H.; Hichwa, B. P. *Thin Solid Films* **1999**, *345*, 312.
(20) Joshi, P. B.; Gelb, A. H.; Malonson, M. R.; Lund, E. L.; Green, B. D.; Silverman, E.; Shinn, E. T.; Long, E. R. In *44th International SAMPE Symposium and Exhibition (Proceedings)*; Society for the Advancement of Material and Process Engineering (SAMPE): Covina, CA, 1999; Vol. I, pp 496−510.

10.1021/cm021752q CCC: $25.00
Published on Web 05/30/2003

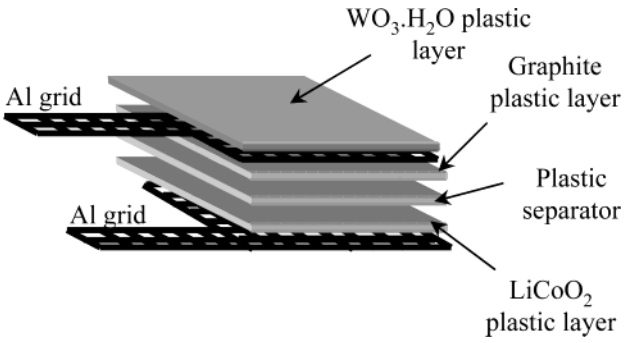

Figure 1. Assembly configuration of the all-plastic electrochromic device. The graphite layer improves the electronic conduction between the Al grid and the $WO_3 \cdot H_2O$ layer. The half-devices studied here were made of the three upper elements.

hydrated tungsten oxide.[21] To reach this flexibility, materials had to be synthesized in powder form before being embedded into a plastic matrix. This procedure led to 50−100-μm-thick plasticized films. The complete battery-like device could then be assembled in an original stack of four of these plasticized layers laminated according to the PLiON technology.[22−24] The surface was able to switch between different reflecting states as a result of the properties of the $Li_xWO_3 \cdot H_2O$ powder embedded in the plastic matrix. It was shown that $Li_xWO_3 \cdot H_2O$ could vary between an isolating (IR nonreflecting) and a conducting (IR reflecting) state depending on the insertion degree x. Thus, hemispherical reflectance over the 2.5−25 μm spectral range was found to vary from 2 to 32% upon intercalation of 0.65 Li^+ ions per tungsten atom in $WO_3 \cdot H_2O$. With these first tests, we demonstrated the feasibility and efficiency of this new original plastic stack for infrared optical switching applications. Nevertheless, it was thought that the reflectance contrast could be improved by modifying the $WO_3 \cdot H_2O$ powder microstructure. In the present paper, we investigated the influence of the $WO_3 \cdot H_2O$ microstructure on the performance of the plastic device as an emissivity modulator.

Experimental Procedure

Preparation of the Devices. The electrochromic devices were fabricated by lamination of several plasticized layers and current collectors as has been described in a previous paper.[21] Thus, half-devices were made with the following successive elements (see Figure 1): (i) an aluminum grid for current collection, (ii) a plasticized layer containing a graphite powder for homogeneous current distribution, and (iii) an electrochromic plasticized layer containing the $WO_3 \cdot H_2O$ powder as the active component powder.

$WO_3 \cdot H_2O$ has an orthorhombic structure (as shown in Figure 2) and belongs to the *Pnmb* space group.[25] $WO_3 \cdot H_2O$ is formed of sheets of distorted octahedral units of tungsten atoms coordinated by five oxygen atoms and a water molecule. The tungsten octahedron shares four corners in the equatorial plane to form sheets. The sheets are linked by hydrogen bonds between the water molecules and the neighboring oxygen atoms of the adjacent layer

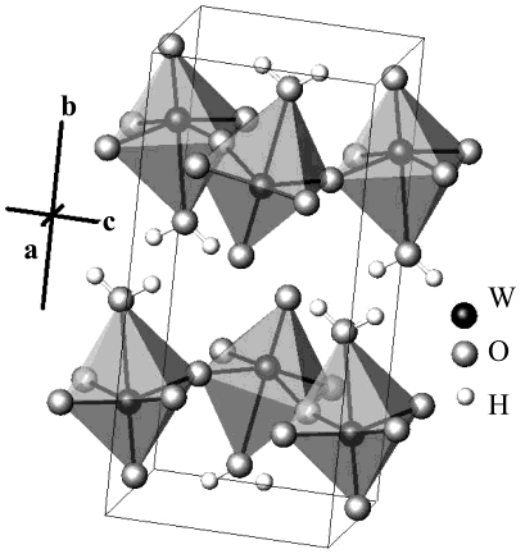

Figure 2. Schematic representation of the $WO_3 \cdot H_2O$ orthorhombic unit cell.

In our first work,[21] the $WO_3 \cdot H_2O$ powder was synthesized according to the Freedman method,[26,27] which is based on a rapid precipitation of the product. According to this route, $WO_3 \cdot 2H_2O$ precipitate is obtained by progressively adding a 1 M $Na_2WO_4 \cdot 2H_2O$ solution (50 mL) to a 3 M HCl solution (450 mL) at 25 °C. After 3 h, the filtered $WO_3 \cdot 2H_2O$ was washed and dehydrated at 110 °C. The crystallite size of $WO_3 \cdot H_2O$ was then about 200 nm. To investigate the influence of the $WO_3 \cdot H_2O$ microstructure on device reflectance, the $WO_3 \cdot H_2O$ powder synthesis was carried out in this study according to a different route described by Furusawa et al.[28] and based on a sol−gel technique.

Crystal growth took longer time using this latter method. According to this approach, 3.5 g of sodium tungstate $Na_2WO_4 \cdot 2H_2O$ was first dissolved in 50 mL of distilled water, and the solution was cooled to 5 °C. Next, 25 mL of 1 M HCl solution cooled to the same temperature was added in one step. The mixture gradually became turbid and, within a few minutes, turned a yellowish gel. Ten hours later, a centrifuge washing procedure was conducted, and the tungstic acid gel was dispersed in 2 L of distilled water. This last turbid solution was allowed to ripen for 15 days. During that time, the tungstic acid gel precipitated, and it was thus easily retrieved by filtration. Depending on the values of the ripening time t and the ripening temperature T, the crystallite length varied from 3 μm (t = 15 days, T = 5°C) to 7 μm (t = 15 days, T = 25°C). Those two criteria (t, T) are of crucial importance in controlling the $WO_3 \cdot H_2O$ microstructure.

Structural Analysis. X-ray diffraction measurements were carried out with a Siemens D5000 diffractometer. SEM measurements were conducted with a Philips FEG (field-effect gun) XL 30 microscope for the Freedman powder and with a Hitachi S2500 microscope for the Furusawa powder and the plasticized films. TEM measurements were made with a JEOL JEM-100CXII microscope using a 120 keV irradiating energy.

Electrochemical Intercalation Procedure. Li-ion intercalation and deintercalation in $WO_3 \cdot H_2O$ were performed using a Mac-Pile system (Bio-Logic, Claix, France) working in potentiodynamic mode. The working electrode was composed of the active layer ($WO_3 \cdot H_2O$) laminated with the aluminum grid and the graphite plasticized layer. Working electrodes were intercalated using metallic lithium as the counter

(21) Bessière, A.; Marcel, C.; Morcrette, M.; Lucas, V.; Viana, B.; Baffier, N.; Tarascon, J.-M. *J. Appl. Phys.* **2002**, *91* (3), 1589.
(22) Bessiere, A.; Beluze, L.; Morcrette, M.; Lucas, V.; Baffier; N. *Solid State Ionics*, in press.
(23) Gozdz, A. S.; Schmutz C.; Tarascon, J.-M. U.S. Patent 5,296,318, 1994.
(24) Tarascon, J.-M.; Gozdz, A. S.; Schmutz, C.; Shokoohi, F.; Warren, P. C. *Solid State Ionics* **1996**, *86*, 49.
(25) Szymanski, J. T.; Roberts, A. C. *Can. Mineral.* **1984**, *22*, 681.
(26) Freedman, M. L. *J. Inorg. Eng. Data* **1963**, *8*, 111.
(27) Freedman, M. L.; Leber, S. *J. Less-Common Metals* **1964**, *7*, 427.
(28) Furusawa K.; Hachisu, S. *Sci. Light* **1966**, *15* (2), 115.

electrode (also used as the reference) in an EC/DMC−$LiPF_6$ (1 M) electrolyte solution in a water-free environment (less than 5 ppm of water). The samples made with the Furusawa powder were electrochemically intercalated as follows: Reduction sweeps were driven by potential cycling with galvanostatic acceleration (PCGA)[29] between 3.5 and 2.1 V. By this method, the electrochemical system is submitted to potential steps. The next step was performed if the previous step time was overrun or if the current decreased below a limit value. Here, the step time and current limits were set to 1 h and *C*/20 so that intercalation could be performed in such a way that the sample was always very close to thermodynamic equilibrium. Four intercalated phases could be distinguished by in situ X-ray diffraction experiments.[22] It was found that, for the Furusawa-type $Li_xWO_3{\cdot}H_2O$ powder, insertion and removal cycles up to $x = 0.35$ (corresponding to the first phase named alpha) were reversible. For higher lithium contents, the insertion was not reversible.[22] Freedman samples were intercalated by a 1 mV/s potential sweep between 3.4 and 1.5 V vs Li^+/Li as previously described.[21] Note that this scan rate was too high for the system to be close to its equilibrium, but the inserted charge could be released at each cycle, and the system was reversible.[21] In each case, the current was integrated to obtain the inserted and extracted *x* values in $Li_xWO_3{\cdot}H_2O$.

Infrared Optical Measurements. Hemispherical reflectance measurements were carried out using two different spectrophotometers, depending on the infrared wavelength domain. The visible/near-infrared range (vis/NIR range = 0.3−2.5 μm) was explored with a Perkin-Elmer Lambda 19 spectrophotometer. The angle of incidence was 8°, and a Spectralon sample (supplied by Labsphere) was used as the reference. Reflectance measurements over the mid-infrared range (mid-IR range = 2.5−25 μm) were performed by using a Nicolet 20 DX spectrophotometer coupled with a homemade optical setting and a bolometer as a weak-signal detector. The thermal detector was kept at low temperature (4.2 K) inside a low-pressure (10^{-5} bar) enclosure to minimize thermal exchange by conduction or convection. Reflectance data were collected at a 25° incident angle. An Al mirror was used as the reference. In each case, measurements were performed ex situ: after cycling, half-devices were removed from the electrolyte solution and transferred to the spectrophotometers. Measurements were then carried out in air on half-cells containing $WO_3{\cdot}H_2O$ intercalated with Li^+. The measurement time was kept below 2 min to minimize spontaneous delithiation in air.

We verified that the $WO_3{\cdot}H_2O$ plasticized layer showed no transmitted light over the entire infrared range. Thus, the optical properties hereafter observed originate from only the $WO_3{\cdot}H_2O$ plasticized top layer. The emissivity could be deduced in the case of lambertian behavior [30] by

$$\epsilon = \frac{\int_{\lambda_1}^{\lambda_2}[1 - R(\lambda)]M_b(\lambda,300)\,d\lambda}{\int_{\lambda_1}^{\lambda_2}M_b(\lambda,300)\,d\lambda}$$

where $M_b(\lambda,300)$ is the blackbody emittance at 300 K. When $R(\lambda)$ is almost constant, the emissivity value can be very simply expressed as $\epsilon(\lambda) \approx 1 - R(\lambda)$.

Results and Discussion

Structures and Microstructures of the $WO_3{\cdot}H_2O$ Powders and Films. Figure 3a shows a SEM micrograph of the $WO_3{\cdot}H_2O$ powder obtained by the Freedman route that reveals 30-nm-thick parallelepiped-shaped grains. A completely different microstructure was achieved using the Furusawa method. With this method,[28] increasing ripening conditions up to 15 days at 25 °C led to the largest grains surface area (Figure 3b). These platelet-shaped grains presented an average surface area of about $5 \times 3\ \mu m^2$. Hence, with this latter method, the grains were up to 1000 times more extended than those synthesized with the Freedman method.

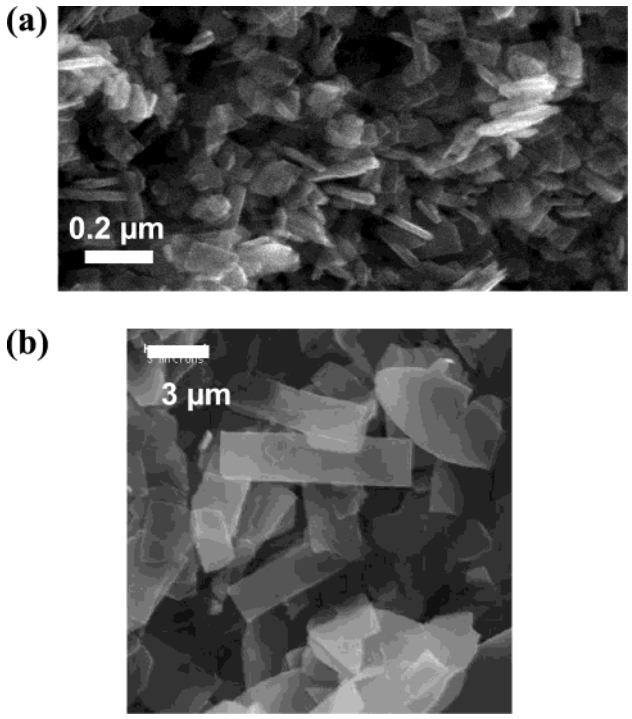

Figure 3. SEM micrographs of the $WO_3{\cdot}H_2O$ powder obtained by the (a) Freedman procedure ($T_{ambient}$, 3 h) and (b) Furusawa process (T = 5 °C, gel ripened at 25 °C for 15 days).

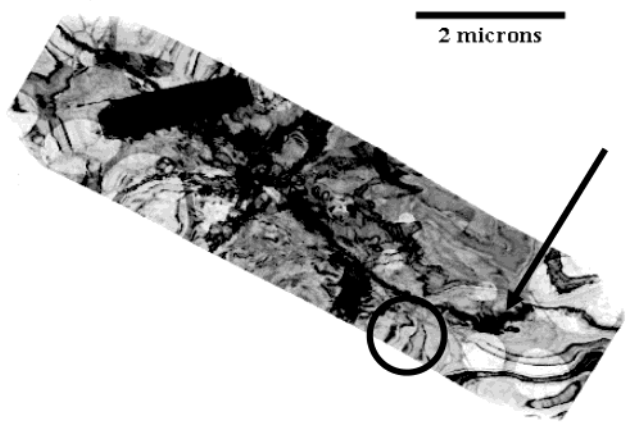

Figure 4. TEM image of a $WO_3{\cdot}H_2O$ grain synthesized by the Furusawa procedure. The arrow indicates an unbroken bend contour. One can follow this bend contour from one side to the other side of the particle, indicating that the particle is monocrystalline. The circle points out the presence of dislocations, where the bend contours are broken.

TEM experiments carried out on the large grains demonstrated, as expected, that the platelets have grown in the *ac* plane.[31] In Figure 4, bend contours can be distinguished as unbroken lines, indicating that the $WO_3{\cdot}H_2O$ grains are monocrystalline. This feature is a priori beneficial in applications because the fewer the

(29) Chabre, Y. *Chemical Physics of Intercalation;* Bernier, P., Ed.; Plenum Press: New York, 1993.

(30) Touloukian, Y. S.; DeWitt, D. P.; Hernicz, R. S. *Thermophysical Properties of Matter*; IFI/Plenum Press: New York, 1972; Vol. 9: Thermal Radiative Properties of Coatings.

(31) Marty, L. Ph.d. Thesis, Université Pierre et Marie Curie−Paris VI, Paris, 1972.

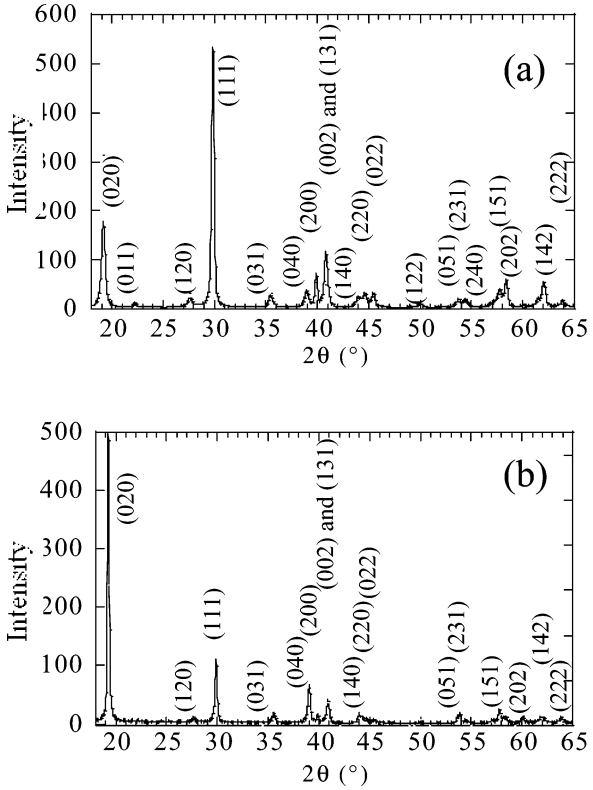

Figure 5. X-ray diffraction patterns of $WO_3 \cdot H_2O$ powders synthesized by the (a) Freedman and (b) Furusawa procedures.

crystalline defects, the higher the free electron mobility in the intercalated state, and hence, the higher the reflectance values. TEM images also testify to the presence of dislocations (circled in Figure 4) that could slightly lower the free electron mobility in the intercalated samples. The grain thickness was evaluated to be about 40 nm according to TEM cross-section images.

X-ray diffraction measurements carried out on the $WO_3 \cdot H_2O$ powders synthesized by the two different methods are presented in Figure 5. Differences between the two microstructures result in different relative intensities for the (0*k*0) diffraction peaks in comparison to the (*hkl*) peaks, where *h* and/or *l* are not equal to 0. The (020) and (040) peaks are particularly intense for the large grains (see Figure 5b), indicating that platelet-shaped grains are lying on the sample-holder substrate.

Microstructure characterization experiments were then carried out on the plasticized films themselves prepared from the two different $WO_3 \cdot H_2O$ powders. The X-ray diffraction measurements on the plasticized films led to somewhat the same features as in the case of the corresponding powders (i.e., before introduction in the films). With the platelet-shaped grains, the (0*k*0) peaks were actually much more intense than the other peaks, whereas the usual relative intensities were observed with the smaller parallelepiped grains. This means that these grains have a random orientation within the plastic matrix, whereas the platelet-shaped grains are parallel to the plastic film surface. This information can be visualized by scanning the film surface by means of electronic microscopy. For the Furusawa-type powder, the $WO_3 \cdot H_2O$ grains are all oriented toward the surface, as their platelet shape can be distinguished in the SEM image (Figure 6a). Hence, the film surface seems to be paved with grains stuck together by the plastic matrix.

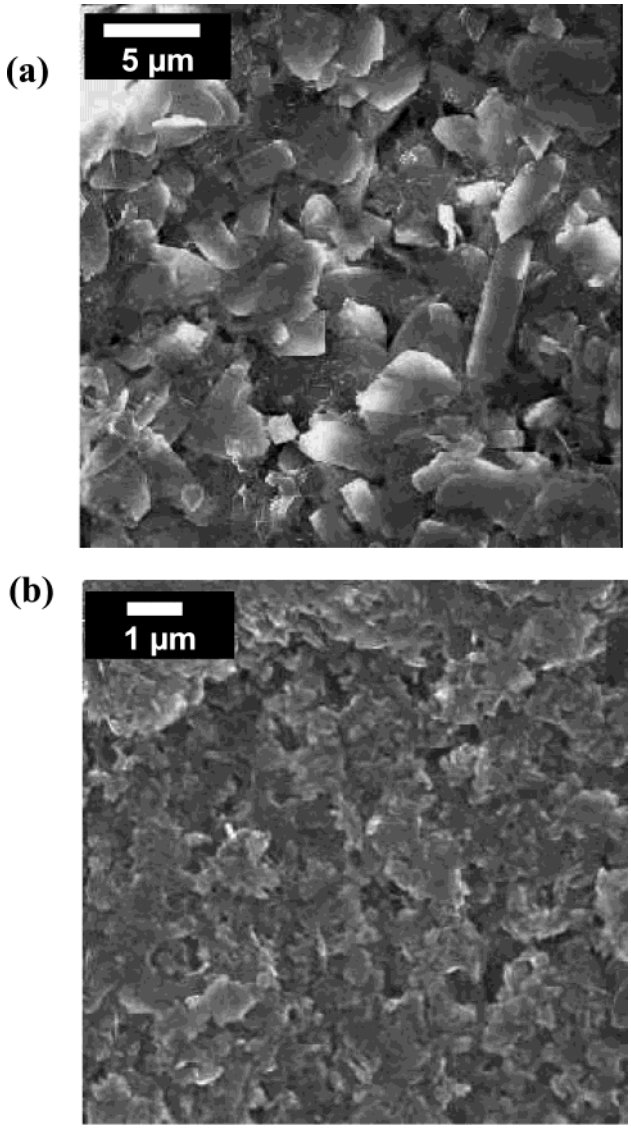

Figure 6. SEM micrographs of the active powder ($WO_3 \cdot H_2O$) embedded in the polymer in the case of synthesis by the (a) Furusawa and (b) Freedman procedures.

On the contrary, the $WO_3 \cdot H_2O$ grains cannot be well distinguished on the SEM image for the Freedman preparation (Figure 6b). Only pores created in the PVDF−HFP polymer by the DBP extraction during the films preparation step can be observed.

To this point, we can highlight two main differences in plastic samples made with the two different powders: (i) the size of the crystallites themselves and (ii) the orientation of the grains within the plastic matrix due to crystallite size. Both of these features strongly influence the optical properties of the devices.

Optical Properties of the Devices. Plastic half-cells were built as described in the Experimental Procedure section. Reflectance measurements were carried out over the 0.3−2.5 μm (NIR) spectral range, as well as over the 2.5−20 μm (mid-IR) spectral range. In the following section, the results obtained over the two ranges are combined on the same graph for convenience.

The reflectance spectra of unintercalated half-cells made using the two different microstructure shapes of the $WO_3 \cdot H_2O$ active component are reported in Figure 7. The spectra clearly differ depending on the micro-

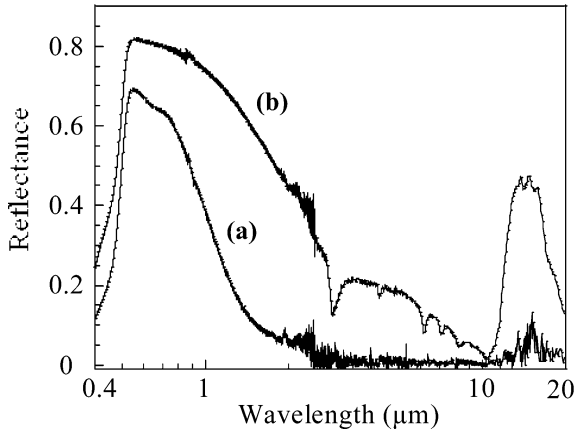

Figure 7. Hemispherical reflectance spectra of unintercalated (oxidized) half-cells made with the (a) Freedman and (b) Furusawa microstructures over the vis/NIR and mid-IR spectral ranges.

structure. In the shorter-wavelength part of the spectrum ($\lambda < 0.5$ μm), light is absorbed through the fundamental absorption of $WO_3 \cdot H_2O$. This blue-light absorption is responsible for the intense yellow color observed for the unintercalated $WO_3 \cdot H_2O$ plastic films. As expected, this absorption is located roughly at the same wavelength, around 400 nm, regardless of the microstructure, since it is related to the band gap of the material.[32]

Beyond 0.5 μm, a strong reflection can be observed in the spectra in Figure 7. Notice that some small and narrow absorption peaks visible at 2.9, 4.3, 6.2, 7.2, and 8.2 μm can be observed in Figure 7b. These extra peaks most likely correspond to absorption, in ambient atmosphere, of air molecules (mainly CO_2 and H_2O). The fact that the strong reflection decreases with wavelength is attributed to light scattering by $WO_3 \cdot H_2O$ particles that takes place when the incident wavelength has a value close to the particle size. The large difference in the particle microstructure of the two powders therefore explains the difference in reflectance spectra between 0.5 and 8 μm: the scattering phenomenon vanishes beyond 2 μm for small-grained films, whereas a scattering reflectance tail can still be observed up to 8 μm for the larger grains.

Furthermore, another strong reflection band can be observed between 11 and 20 μm, especially for one type of microstructure. This characteristic feature was assigned to the $WO_3 \cdot H_2O$ restrahlen band of the compound, originating from the interaction between the incident light and the phonon lattice of the crystal.[33] To our knowledge, this kind of observation has never been observed for crystalline $WO_3 \cdot H_2O$ lattice. Nevertheless, the phenomenon was noticed by Georg et al.[34] for *m*-WO_3 films. Longitudinal (λ_L) and transverse (λ_T) phonon optical modes were then situated at 970 cm^{-1} (10.3 μm) and 640 cm^{-1} (15.6 μm), respectively. Note that the restrahlen band for the large platelets is much more pronounced than that for smaller grains. Two main reasons can be given for this:

(i) The $WO_3 \cdot H_2O$ crystalline domains are much wider for large grains, hence leading to a higher phonon density within the compound. Coupling of the electromagnetic incident wave with the phonon lattice is therefore more efficient, inducing a higher reflectance intensity.

(ii) The difference in the two spectra can be related to the strong preferential orientation of the platelet-shaped grains compared to the random orientation of the small parallelepiped grains. Indeed, in the case of the larger grains (Furusawa preparation procedure), the transverse optical phonon modes of $WO_3 \cdot H_2O$ have the same orientation for all grains with respect to the incident transverse electric field vector. They are all excited for the same incident direction, hence leading to a high reflectance. On the contrary, only a part of the phonon optical modes in the smaller grains (Freedman preparation procedure) are fully efficient in interacting with the incident light.

Considering unintercalated samples, the reflectance results indicate that small parallelepiped grains are preferable.

Reflectance measurements were then carried out on intercalated half-cells. Li^+ intercalation was performed as described in the Experimental Procedure section. Recall that $WO_3 \cdot H_2O$ switches from an insulator to a metal-like compound as Li^+ ions are inserted. Upon Li^+ intercalation, $WO_3 \cdot H_2O$ is reduced, and added electrons fill the previously empty conduction band, providing metallic properties to the material according to the Drude model.[35]

Figure 8 shows reflectance (Figure 8a) and emissivity (Figure 8b) spectra (0.3−2.5 and 2.5−20 μm, respectively) of some intercalated plasticized films with different $WO_3 \cdot H_2O$ microstructures. The Li content within the samples corresponds to the highest reflectance that could have been obtained for each microstructure. The Li^+ insertion content is significantly lower for the microstructure obtained by the Furusawa procedure since intercalation was conducted much closer to thermodynamic equilibrium (see Experimental Procedure section). First, the fundamental absorption is almost not observable over the 0.3−20 μm spectral range. We can distinguish a portion of this absorption band for wavelengths shorter than 0.4 μm (see Figure 8). Therefore, the optical band gap of intercalated $Li_xWO_3 \cdot H_2O$ was roughly evaluated to be 0.25 μm (5 eV). As for *m*-WO_3,[36] the band gap was found to increase with cation intercalation and tungsten reduction. Beyond these wavelengths in the spectra, a reflection band can be observed for $\lambda < 0.5$ μm. As for the unintercalated samples, this reflectance is ascribed to light scattering by the $Li_xWO_3 \cdot H_2O$ particles. However, the phenomenon is now partly hidden by a large absorption band centered around 0.8 μm and originating from damping of the free electron motion according to the Drude model. Furthermore, scattering reflection might be lower for the intercalated samples than for unintercalated ones simply because of the variation in the material refractive index. These features give the dark blue color to the film. The reflectance raising from 1 μm and the subsequent high

(32) Svensson, J. S. E. M.; Granqvist, C. G. *Appl. Phys. Lett.* **1984**, *45* (8), 828.
(33) Kittel, C. *Physique de l'Etat Solide*, 5th ed.; Dunod Université: Paris, 1983.
(34) Georg, A.; Graf, W.; Wittwer, V. *Sol. Energy Mater. Sol. Cells* **1998**, *51*, 353.
(35) March, N. H.; Parrinello, M. *Collective Effects in Solids and Liquids*; A. Hilger: Bristol, U.K., 1982.
(36) Green, M.; Hussain, Z. *J. Appl. Phys.* **1993**, *74*, 5.

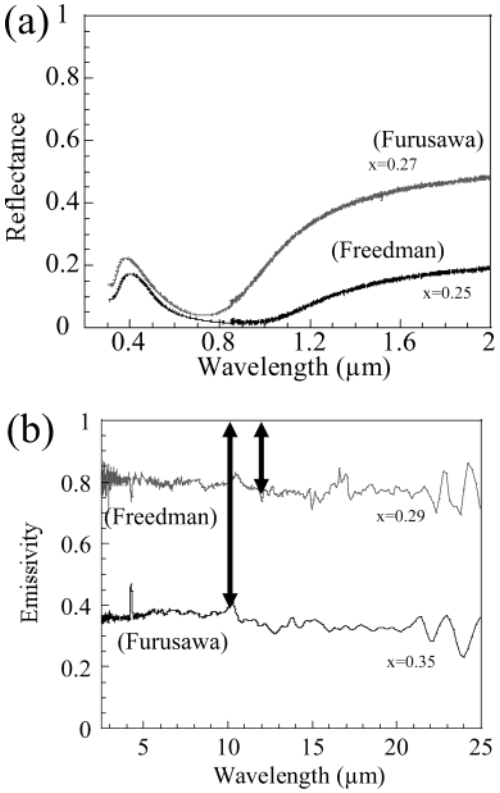

Figure 8. Hemispherical reflectance spectra of intercalated (reduced) half-cells made with the Freedman and Furusawa microstructures over the (a) vis/NIR and (b) mid-IR spectral ranges. Arrows represent the emissivity contrasts obtained for the two microstructures at about 10 μm (see Figures 7 and 9 for the unintercalated infrared optical spectra).

reflectance plateau are ascribed to the free electrons of the intercalated compounds and are well described by Drude behavior.[35] As the plateau extends into the infrared range and especially throughout interesting ranges from the application point of view (i.e., 3−5 and 8−12 μm for camouflage application, for instance), the reflectance value reached on this plateau is of particular interest: indeed, the highest possible reflectance is required. Figure 8 shows that large-grained microstructure clearly leads to higher reflectance between 2 and 20 μm than the smaller-grained microstructure. This phenomenon might originate from three factors:

(i) First, the numerous grains boundaries (and possibly the presence of other defects) might be responsible for free electron scattering and, therefore, for a lower free electron mobility. In contrast, when the active $WO_3 \cdot H_2O$ powder is composed of monocrystalline grains 3 orders of magnitude larger, greater mobility for the free electrons in the intercalated samples is guaranteed. As expressed by the Drude model, the higher the mobility is, the higher the reflectance will be.

(ii) Furthermore, the $WO_3 \cdot H_2O$/polymer ratio at the film surface might differ depending on the microstructure (see Figure 6). Higher ratios are observed for the larger grains because of the lamination procedure, and this could be responsible for the higher reflectance values.

(iii) Finally, the strong preferential orientation of the platelets compared to the random orientation of the small parallelepipeds likely explains the stronger reflection values obtained for a given light incidence. Considering the low-dimensionality structure of $Li_xWO_3 \cdot H_2O$, electron gas oscillations in the sheet planes should induce stronger coupling with an electric field oriented parallel to these sheets. This is actually the case for reflectance measurements carried out on samples obtained by the Furusawa procedure, since the incidence angle is close to the normal (i.e., 8° away from normal) and $WO_3 \cdot H_2O$ sheet planes are roughly parallel to the sample surfaces. On the contrary, the parallelepipeds obtained by the Freedman procedure have a random orientation with respect to the surface of the samples. Therefore, coupling of a transverse electric field with the electron gas can be more or less favorable, depending on the orientation of each grain.

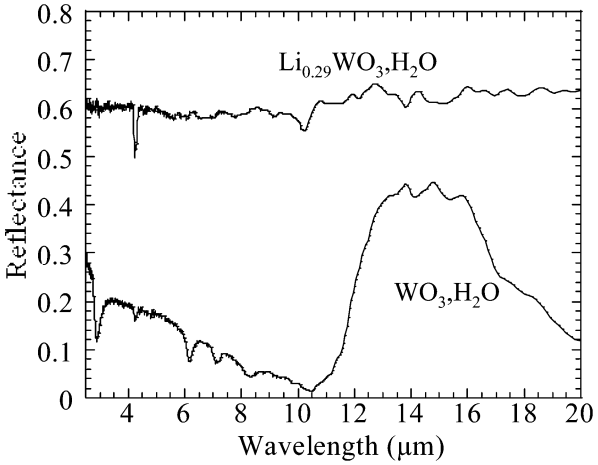

Figure 9. Hemispherical reflectance spectra of unintercalated and intercalated half-cells made with the Furusawa microstructure over the mid-IR spectral range.

To this point, the large-grained microstructure is much more interesting, considering the goal of obtaining the highest reflectance value for intercalated samples. A comparison between the total optical performance characteristics of the two microstructures now appears useful. To highlight the electrochromic performance, Figure 9 displays, in a linear wavelength scale between 2.5 and 20 μm, the reflectance spectra of unintercalated and intercalated samples. One can extract from these spectra some reflectance contrast values over several significant spectral ranges. Thus, for instance, 41 and 53% contrasts are found over the 3−5 and 8−12 μm spectral ranges, respectively (reflectance difference taken between unintercalated and intercalated samples). More contrast values are given in Table 1 for both microstructures. As reported, the large-grained microstructure of the $WO_3 \cdot H_2O$ active powder appears much more favorable for obtaining higher reflectance contrast. The performances are somewhat hindered by the short-wavelength scattering phenomenon for the 3−5 μm range and by the restrahlen phenomenon for the 8−12 μm range. Finally, an average 61% highest reflectance value over 2.5−20 μm can be achieved for the intercalated material. This roughly equals the 60% value obtained at 2.5 μm by Goldner et al,[10] yet working on a rigid and much heavier device based on *m*-WO_3. Another comparison is relevant: an average 42% reflectance contrast between 4 and 16 μm was found here, comparing favorably to the average 35% found by Cogan et al.[14] for a rigid *m*-WO_3-based system. Another important point is the optical reversibility. For the $WO_3 \cdot H_2O$

Table 1. Reflectance Contrasts between $WO_3 \cdot H_2O$ and $Li_xWO_3 \cdot H_2O$ for the Freedman-type ($x = 0.65$) and Furusawa-type ($x = 0.29$) Films over Different Spectral Ranges[a]

	3−5 μm	8−12 μm	2.5−10 μm	2.5−20 μm	2.5−25 μm
Freedman microstructure	0.26 (0.27/0.01)	0.29 (0.30/0.01)	0.27 (0.28/0.01)	0.26 (0.30/0.04)	0.28 (0.32/0.04)
Furusawa microstructure	0.41 (0.60/0.19)	0.53 (0.58/0.05)	0.48 (0.60/0.12)	0.42 (0.61/0.19)	0.43 (0.61/0.17)

[a] Maximum/minimum values are also indicated for each spectral range.

dispersed small grains, the reversibility is quite good, and after several electrochemical cycles, the optical response is comparable to the first lithium insertion.[21] For the large $WO_3 \cdot H_2O$ grains, the optical contrast of the deintercalation step for the first cycle is limited to 30%. Indeed, the grain morphology in the large platelets seems less favorable than that in the smaller grains with respect to lithium intercalation. Further studies after several intercalation−deintercalation cycles have to be performed to confirm this behavior.

Conclusions

All-plastic electrochromic devices were fabricated following previously developed procedures, i.e., using a $WO_3 \cdot H_2O$ powder embedded in a plastic matrix. In this study, the emphasis was on the microstructure of the $WO_3 \cdot H_2O$ powder in view of improving the device performance. Thus, two synthesis methods (the Freedman and Furusawa routes) were used, as they lead to very different shapes of particles. The Furusawa synthesis is based on the slow growth of crystallites. With this approach, large platelet-shaped grains were obtained instead of the small parallelepiped-shaped grains previously obtained with the Freedman procedure. It was discovered that the powder microstructure remains the same in the plastic matrix and is of crucial importance for optical results: it greatly modifies the reflectance spectra for unintercalated as well as intercalated samples. The larger grain size of the Furusawa powder ($5 \times 3\ \mu m^2$) was found to induce a much higher intensity for free electron reflectance above the plasma wavelength. Thus, an average contrast as high as 53% for the 8−12 μm range was measured, comparing favorably with the best results obtained for devices presently built on rigid substrates. Emissivity contrasts are about 60 and 20% at 10 μm from the Furusawa- and Freedman-type structures, respectively. Indeed, with the improved $WO_3 \cdot H_2O$ microstructure, the electrochromic device properties are enhanced. We are now working to gain insight into the electrochemical behavior of $WO_3 \cdot H_2O$ by analyzing the reversibility and kinetics of the devices. By investigating the electrochemical insertion phenomenon as related to the optical response of the system, we hope to gain precise control of device reflectance and a better understanding of the relationships between the electronic and optical properties of $Li_xWO_3 \cdot H_2O$.

Acknowledgment. Dr. P. Vermaut is acknowledged for the TEM analysis. The authors are thankful to Prof. N. Baffier and Prof. J. M. Tarascon for fruitful discussions.

CM021752Q